Digest Journal of Nanomaterials and Biostructures Vol. 19, No. 4, October-December 2024, p. 1591-1603

Impact of fly-ash (silica) on amorphous phase formation in $NaNO_3$-$Sr(NO_3)_2$ composite solid electrolytes

T. V. Kumar [a,*], M. C. S. Reddy [b], G. Prathibha [b], B. H. C. Rao [c], J. V. Kumar [d], P.S. Kumar [e]

[a] *Department of Physics, CVR College of Engineering, Hyderabad, India.*
[b] *Department of Physics, CMR College of Engineering & Techonology, Hyderabad, India*
[c] *Department of Physics, Gokaraju Rangaraju Institute of Engineering and Technology, Hyderabad, India*
[d] *Department of H&S, SKU College of Engineering & Technolog, Sri Krishnadevaraya University, Anathapur, A.P., India*
[e] *Dept. Of Physics, St.peter's Engineering College,Hyderabad, India*

In the current research, various weight percentages of flyash were incorporated into a mixed system of 85.32% $NaNO_3$ and 14.68% $Sr(NO_3)_2$. The system was analyzed using the studies of conductivity, dielectric and electric modulus. An increase in DC conductivity was observed with the addition of flyash, peaking at 10% by weight. Beyond this concentration, the conductivity began to decrease. This increase in conductivity is attributed to the formation of an amorphous phase within the mixed sytem. XRD, FTIR, SEM, and DSC analyses of the flyash dispersed systems indicated the formation of an amorphous phase. The amorphous phase may be due to the surface interaction between fly-ash(silica)and phase of mixed system. The AC conductivity, which depends on frequency, adheres to universal power law. Power law parameter were determined.

(Received August 19, 2024; Accepted October 23, 2024)

Keywords: Solid electrolytes, Energy materials, ionic conductivity, Amorphous Phase

1. Introduction

Sodium-ion batteries (SIB's) are emerging as a potential substitution to lithium-ion batteries, particularly due to their potential for lower costs and enhanced sustainability. One area of significant interest is the use of NASICON (Sodium Superionic Conductor) materials as solid electrolytes. Unlike traditional liquid electrolytes, solid electrolytes can offer improved safety and potentially higher energy densities. NASICON materials are particularly attractive due to their excellent sodium-ion conductivity, making them well-suited for this application. Despite their potential, the use of NASICON materials in practical battery systems is still under investigation, and optimization is necessary for their effective implementation. While NASICON materials face challenges when used as cathodes, their role as solid electrolytes holds considerable promise. Continuing advancements in this sector is critical to realizing the full potential of sodium-ion batteries, with an emphasis on developing safer, more efficient, and practical energy storage options [1-2].

For the past thirty years, heterogeneous doping has been utilized to boost conductivity by incorporating dispersions of chemically inert and highly insoluble insulating particles, such as SiO_2, CeO_2, Al_2O_3, ZrO_2, Fe_2O_3, and SnO_2, into slightly ionic conducting materials. The incorporation of nano particles has resulted in a notable increase in conductivity, often improving by 10–30 times of magnitude in various Na^+ ion conducting composite solid electrolyte systems, including NaCl-Al_2O_3, $NaNO_3$-Al_2O_3, and Na_2SO_4-Al_2O_3 [3–9].

* Corresponding author: Physicistvijay1201@gmail.com
https://doi.org/10.15251/DJNB.2024.194.1591

Sodium nitrate, which features a rhombohedral calcite structure with space group R3c, has two molecules per unit cell and undergoes a phase transition at 547 K due to the orientational disorder of nitrate ions. Sodium nitrate is Frenkel defect cationic(Na^+) concductor i.e the mobile ion is sodium [10-12]. To achieve further improvements in ionic transport, a new host matrix system, denoted as $[NaNO_3]_{(100-x)}$– $[Sr(NO_3)_2]_x$, was introduced to replace conventional $NaNO_3$. This new system demonstrated nearly an order of magnitude increase in conductivity compared to pure $NaNO_3$, particularly at a composition of $[NaNO_3]_{85.32}$– $[Sr(NO_3)_2]_{14.68}$. The observed enhancement in conductivity has been attributed to the phase boundaries formed between the coexisting phases in the system [13-15]. To further enhance conductivity in this host system, we explored the dispersion of nano fly-ash particles into the $[NaNO_3]_{85.32}$– $[Sr(NO_3)_2]_{14.68}$ matrix and investigated how conductivity varied with weight percent and temperature.

2. Experimental

The initial host compound used was $[NaNO_3]_{85.32}$– $[Sr(NO_3)_2]_{14.68}$, prepared by mixing analytical grade $NaNO_3$ and $Sr(NO_3)_2$ with a purity of 99.9% in the appropriate stoichiometric ratio to form mixed crystals. These crystals were then ground into a fine powder to serve as the host material. Additionally, high purity ultra-fine insulating fly-ash(composition of SiO_2 & Al_20_3 etc…) was used as the dispersoid material. The mixing of these materials was carried out using mechanical milling in an agate mortar with acetone, and the grinding process was continued for one hour to ensure a homogeneous dispersion of fly-ash particles in the mixture[16].

A hydraulic press was then used to create pellets with dimensions of 12 mm in diameter and 1-2 mm in thickness at a pressure of approximately 0.432 GPa. The pellets were sintered at 200 degrees Celsius for 24 hours. After sintering, the pellets' surfaces were polished, and silver paste was added to make sure proper electrical contact before mounting them in the sample holder.

The Novo control Alpha-A frequency analyzer was used to perform complex impedance measurements throughout a frequency range of 1 Hz to 10 MHz and a temperature range of 303 to 563 K with 5 K intervals. X-ray diffraction patterns were produced at a scanning angle of 0° to 60° using a Rigaku X-ray diffractometer equipped with Cu-K Alpha radiation at room temperature. SEM and energy-dispersive X-ray analysis (EDAX) were carried out with JEOL JSM 5600 and ZEISS EVO 18. DSC measurements were performed using a PC-based differential calorimeter at a heating rate of 10 °C/min from 323 to 603 K. Using a Bruker infrared spectrometer, FTIR spectra were collected between 400 and 4000 cm−1.

3. Results and discussion

3.1. X-ray diffraction (XRD)

The X-ray diffraction (XRD) patterns for $[NaNO_3]_{85.32}$– $[Sr(NO_3)_2]_{14.68}$ (host), Fly-ash, and various dispersed systems with different weight ratios (w/o) of Fly-ash are presented in Figure. 1. The XRD pattern for the host and composite systems display sharp and intense peaks, confirming its crystalline nature. Conversely, the Fly-ash pattern shows a broad, prominent peak and a significant background, indicating that the fly-ash particles are in the nanometer range [17, 18]. For all dispersed systems, a decrease in peak intensity is observed relative to the host system. This decrease is related to the distribution of the host across the extensive surface area of the fly-ash [19, 20]. Such distribution effects are more prominent when the adhesion energy of the salt exceeds the surface energy of the mobile species. Furthermore, all composite systems with fly-ash exhibit broadening of the prominent peak, which indicates a reduction in the average crystalline dimension or crystallinity of the host with varying fly-ash content [21]. In the system with 10 wt% fly-ash, the characteristic peaks (1 0 4) and (0 1 8) are the only ones that remain sharp, while other peaks show a significant decrease in crystallinity. This suggests that the average crystallite size decreases up to 10 wt% fly-ash before increasing again. The sharp peaks combined with a strong background at 10 wt% fly-ash suggest a mixture of amorphous and crystalline phases, reflecting a

reduction in overall crystallinity. The widening seen at 10 wt% fly ash suggests the presence of very tiny crystallites.

XRD results reveal that tiny crystallites in the host system spread across the fly-ash's vast surface area. The gradual increase in this spreading effect up to the 10 wt% fly-ash threshold signifies the formation of an amorphous phase [22].

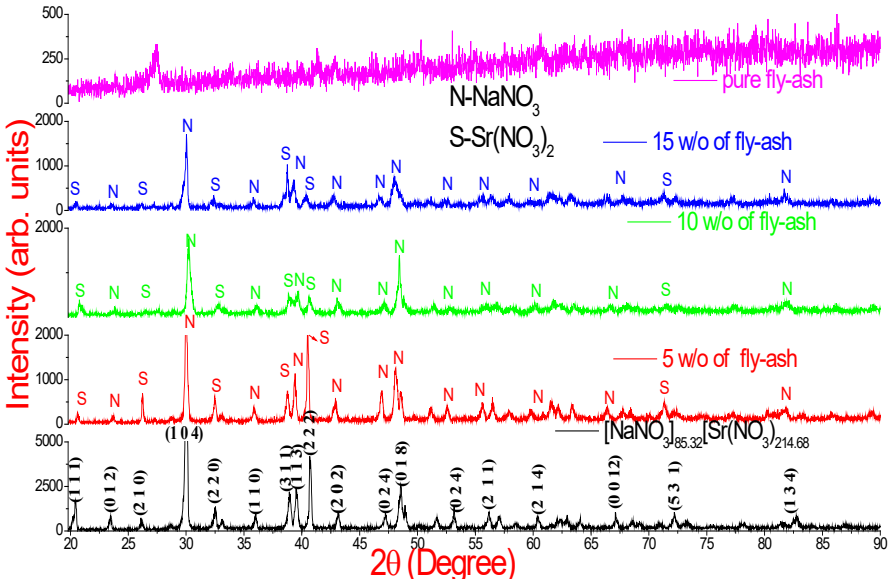

Fig. 1. XRD patterns of host , fly-ash and dispersed systems with different w/o fly-ash.

3.2. Fourier transform infra-red spectroscopy (FTIR)

In Figure 2, the FTIR spectra of the host, fly-ash, and dispersed systems with varying weights of fly-ash (w/o) are illustrated. The existence of nitrate ions in the host system is confirmed by using the basic vibration modes at 835 cm^{-1} (υ2), 1385 cm^{-1} (υ3), and 735 cm^{-1} (υ4). Specifically, The pronounced peak at 835 cm^{-1} is caused by nitrogen vibrations within and outside the NO_3 plane, also known as the NO_3 out-of-plane bending mode. The broad absorption at 1385 cm^{-1} is related with the asymmetric stretching mode of the N-O bond. The weaker band at 735 cm^{-1} corresponds to the doubly degenerated O-N-O bending or the asymmetric in-plane bending mode [23-24].

In the pure fly-ash spectrum, broad absorption bands are observed at 1093 cm^{-1}, 795-800 cm^{-1}, and 461-468 cm^{-1}, which are related to the asymmetric, symmetric, and bending modes of the Si-O-Si bonds in the tetrahedral network, respectively, indicating the presence of silica. Another wide peak at 3641 cm^{-1} is assigned to hydroxyl vibration mode, while the small peak at 557 cm^{-1} is related to the alumina octahedral structure, indicating the presence of alumina [25]. The FTIR spectrum also reveals dehydrated O-H groups on the outer layer of nano-fly-ash particles and confirms the major compounds as silica and alumina [23-26].

In the dispersed systems, the band at 795 cm^{-1}, present in the fly-ash spectrum, is no longer observed. This disappearance suggests a disturbance in the initial order of the fly-ash [20]. The strong peak for the asymmetric stretching of N-O at 1385 cm^{-1} in the host system broadens and shifts to a lower intensity and wave number (1365 cm^{-1}) as the w/o fly-ash increases, indicating a decrease in the crystallinity of the samples. Additionally, bands at 735 and 2447 cm^{-1} in the host system, and at 461 cm^{-1} in fly-ash, slightly shift towards lower frequencies in the dispersed systems. The intensity of the bands at 2766 and 2852 cm^{-1} diminishes with increasing w/o fly-ash. Notably, the out-of-plane bending mode of NO3 (υ2) and υ2 + υ1 in the 10 w/o fly-

ash dispersed system exhibits the highest intensity among all dispersed systems, suggesting a strong interaction between the fly-ash and the host system, which may lead to the formation of an amorphous phase [26].

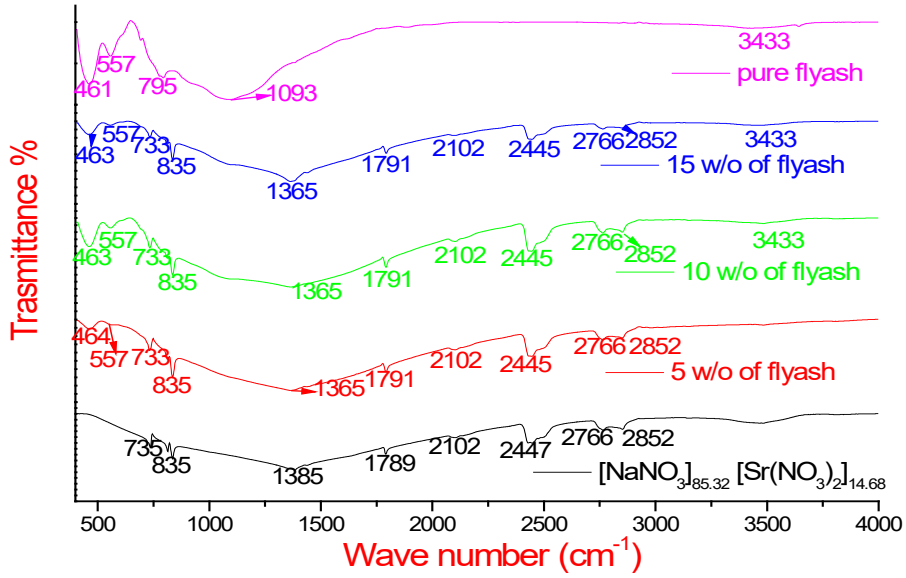

Fig. 2. FTIR spectra of host, fly-ash and dispersed systems with different w/o fly-ash.

3.3. Differential scanning calorimetry(DSC)

DSC peaks for both the host and those with 10% and 15% fly-ash additions are presented in Figure 3. The host system shows a single endothermic peak at 545 K, corresponding to a transition, and another peak at 572 K associated with its melting point [5,11]. Adding fly-ash does not significantly alter the transition temperature but does introduce a minor distortion at the higher temperature end of the peak. Notably, the intensity of the transition peak decreases with increasing fly-ash content, and it eventually disappears at higher concentrations of fly-ash. The melting peak intensity also diminishes significantly, with a reduction of approximately 53% for 15% fly-ash and 76% for 10% fly-ash compared to the host system. This sharp decline in the endothermic peak intensity may be attributed to the development of an amorphous phase [27]. The correlation between these DSC and XRD measurements support the conclusion of an amorphous phase formation.

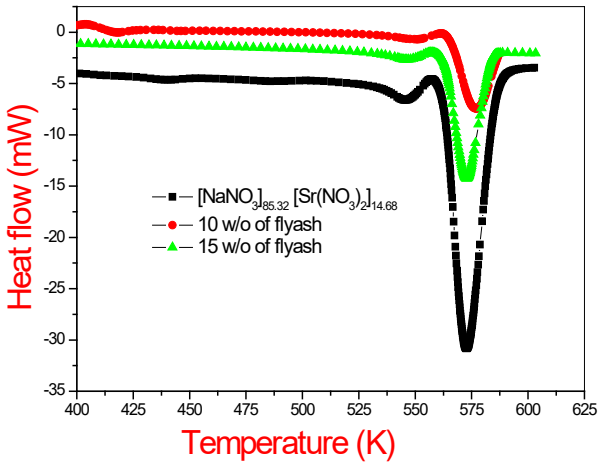

Fig. 3. DSC of host and composite systems with different w/o fly-ash.

3.4. Scanning electron microscope (SEM)

Figure 4 and Figure 5 exhibit SEM and EDAX images of both host and dispersed systems with varying concentrations of fly-ash. As depicted in figure., the grains and their sizes in the host are easily observable, with grains of uneven sizes dispersed throughout the sample. Smaller grains, identified as $Sr(NO_3)_2$, are interspersed among the $NaNO_3$ grains, indicating a two-phase small crystallite structure in the host. The morphology pictures of the fly-ash dispersed system in figure reveal a reduction in grain size compared to the host and a more even dispersion of fly-ash within the host. Additionally, Figure 5 shows some partial amorphous characteristics at a 10 w/o fly-ash concentration. At higher fly-ash concentrations, as seen in Figure 4c, agglomeration of particles is evident. SEM images highlight a good surface interaction between fly-ash and distinct amorphous phases.

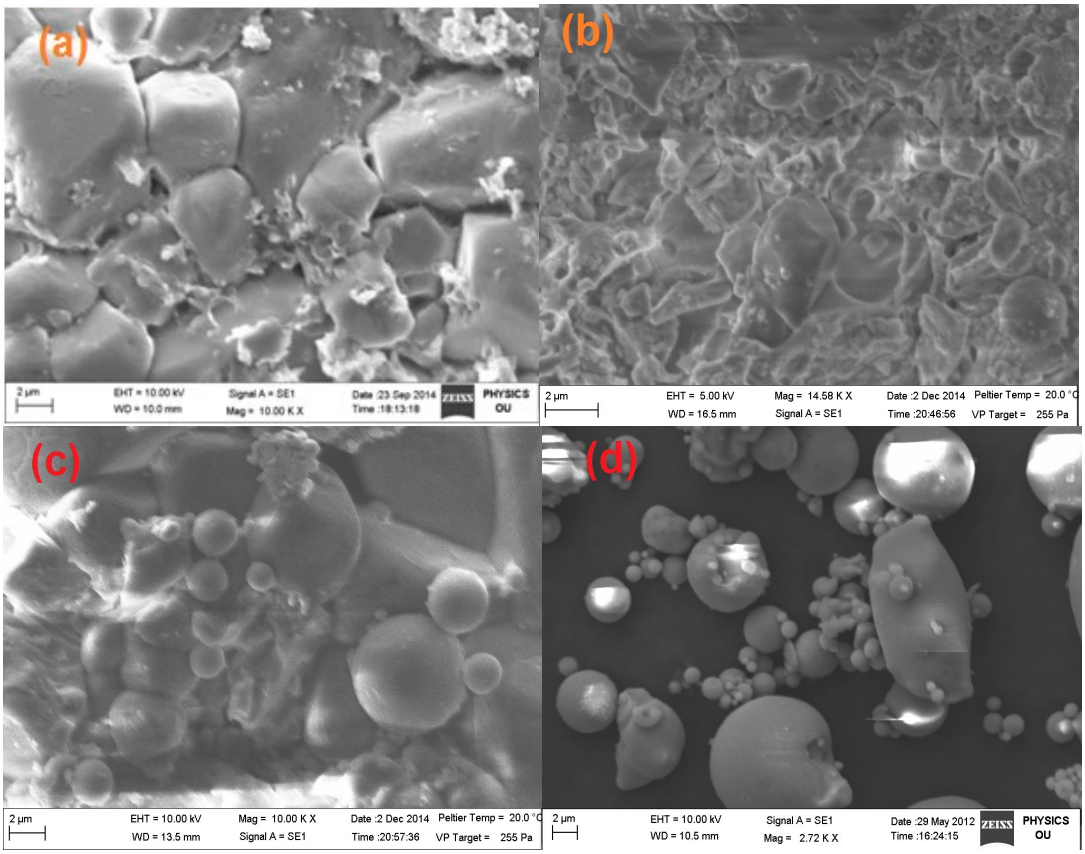

Fig. 4. SEM pictures for (a) host (b) 10 w/o, (c) 25 w/o and (d) pure fly-ash.

Figure 5 displays the EDX spectra for both the host and dispersed systems with fly-ash. The EDX analysis indicates the existence of major atoms such as Na, Sr, N and O in the host system, with additional elements like Si, Al, Nb, Au, and Ta appearing in the dispersed systems. These elements correspond to the components of $NaNO_3$, $Sr(NO_3)_2$, SiO_2, and Al_2O_3 etc . The EDX spectrum of the fly-ash shows prominent peaks for Silicon, Oxygen, and Aluminum

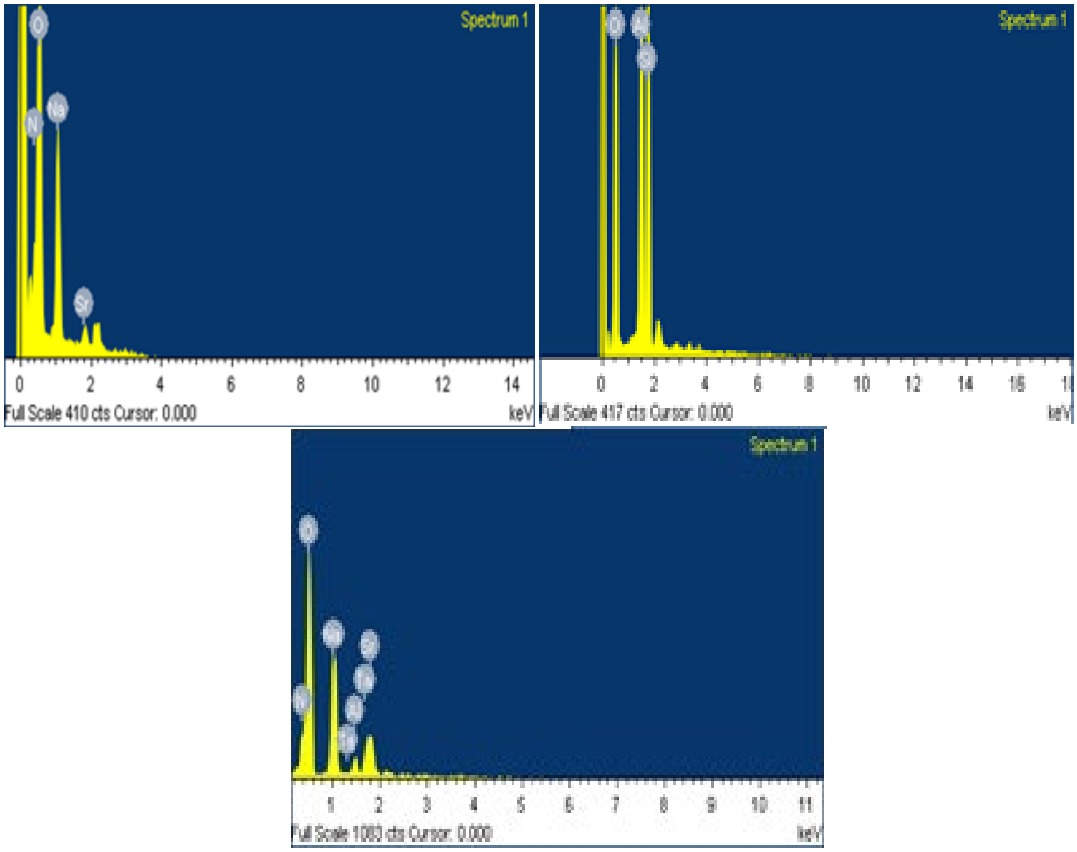

Fig. 5. EDX pictures of host, 10 w/o fly-ash and pure fly-ash, respectively.

3.5. Dielectric study

Figure 6 illustrates the changes in the (a) ε′ and (b) ε″ (c) tan δ with frequency (f) at various temperatures for 10 w/o fly-ash composite solid electrolyte system. At low frequencies, a high ε′ value is observed, which decreases exponentially as the frequency increases. This high ε′ values for small frequencies, regardless of temperature, is related to polarization of space charges. The log f vs. log ε″ plot indicates that mobile ions drive dc conduction, with slopes ranging from −0.7 to −0.98 (near to −1). The slope's divergence from unity may be due to space charge effects at lower frequencies and temperatures. Furthermore, log ε″ progressively increases at lower temperatures, but abruptly increases from 423 K onward due to thermally induced imperfections [28-30]. Peaks in tan δ, at low frequencies shift to higher temperatures as the frequency increases, and peak maximum of tanδ suddenly increases for higher temperatures as a result of increased hopping of charge carriers [30]. The maximum frequency, f_{tan}, temperature as a variable, obey's the exponential behaviour. The activation energy was found to be 1.08 eV between 473 K and 563 K for the 10 w/o fly-ash. This activation energy value is consistent with those obtained from conductivity values computed from the slope of the log ($f_{tan}T$) vs. 1000/T plot (Figure 4(c)),for 10 w/o fly-ash dispersed system.

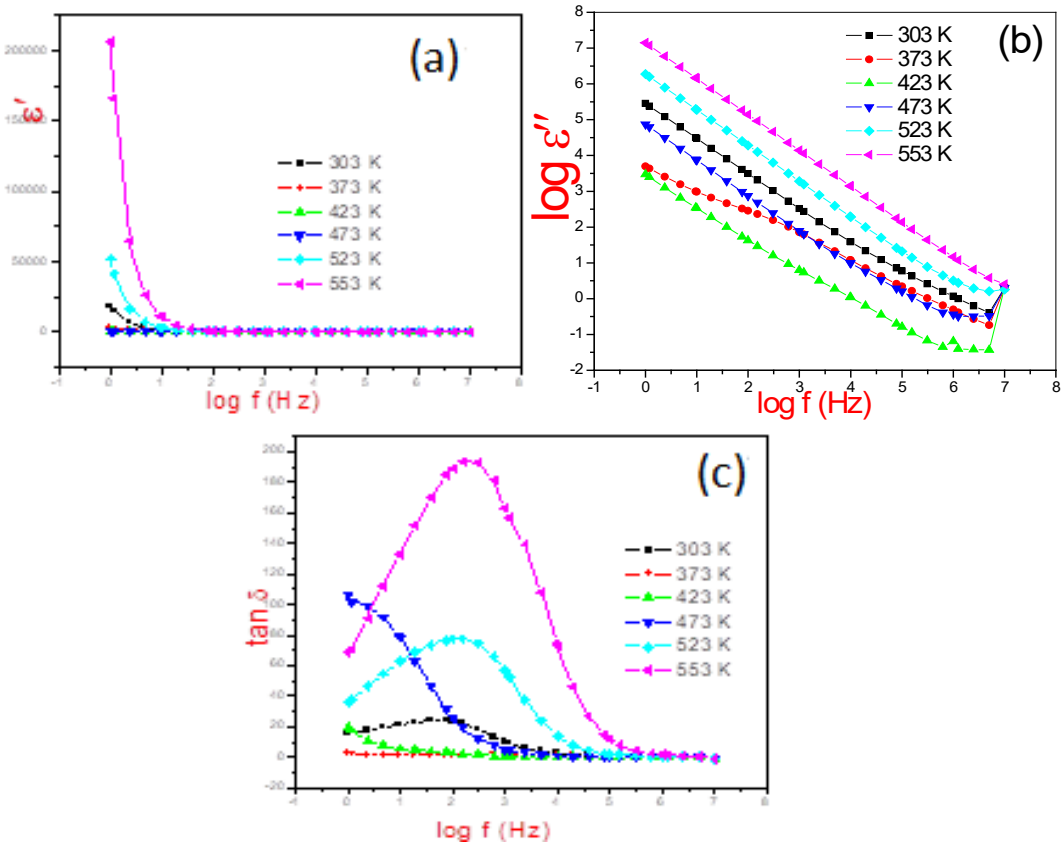

Fig. 6. Frequency dependence of (a) real part (ε') (b) imaginary part (ε") and (c) tanδ for 10 w/o fly-ash at different temperatures.

In Figure 7, the ε′ variation with frequency at 523 K for various fly-ash concentrations is shown. It is evident that ε′ is higher in dispersed systems compared to the host system, with the maximum value observed in the 10 w/o fly-ash composite. This increased ε′ in dispersed systems is likely due to enhanced charge accumulation at the interfaces, leading to higher ionic conductivity [31].

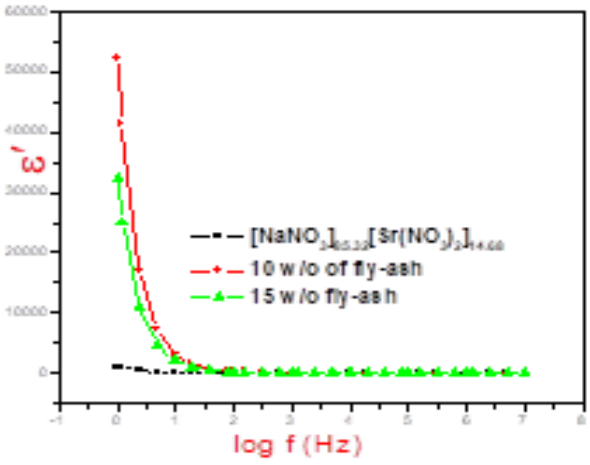

Fig. 7. Variation of ε' with frequency for different w/o fly-ash.

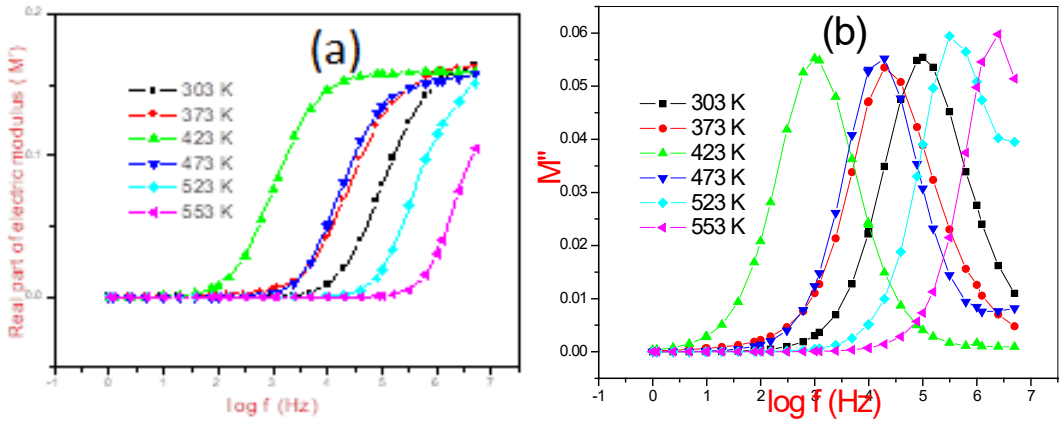

Fig. 8. Variation of (a) M' (b) M" with frequency for 10 w/o fly-ash at different temperatures.

Table 1. Activation energies of host and dispersed systems of fly-ash from electric modulus, dielectric and conductivity data.

w/o fly-ash	Activation energy (eV)			
	DC conductivity	AC conductivity	Dielectric loss (tan δ)	Electric Modulus
0	1.17	1.19	1.05	1.04
5	1.09	--	--	--
10	0.91	1.01	1.08	1.07
15	0.97	1.13	1.22	1.22
20	0.99	1.47	--	--

The changes in real part of electric modulus (M′) with frequency at distinct temperatures for 10 w/o dispersed fly-ash system is shown in Figure 8 (a). The M' values approach zero at lower frequencies across all temperatures, indicating minimal electrode-electrolyte interface polarization, as observed in the dielectric constant and loss. As frequency increases, M' shows dispersion and reaches a maximum for higher frequencies.

Figure 8 (b) illustrates the changes in imaginary part of electric modulus (M") with frequency for varios temperatures. A wide maximum is visible towards the higher frequencies at all temperatures in the 10 w/o fly-ash system. The increasing trend of M" below the peak maximum at low frequencies represents extended movement of charge carriers, whereas the decreasing trend above the peak indicates confinement of charge carriers to their potential wells, i.e., short-range motion of mobile ions. The maximum value signifies the transition from long-range to short-range motion of mobile ions, indicating conductivity relaxation [32].The frequency at which M" is maximum, $f_{M"}$, represents the most probable relaxation frequency, and its position shifts to greater frequencies with increasing temperature. The relationship between $f_{M"}$ and temperature follows the Arrhenius equation and activation energies were computed. Table 1 shows that these activation energies are consistent with those obtained from dielectric and conductivity studies, suggesting a hopping mechanism in the samples [33].

3.6. Conductivity study

Figure 9 illustrates the logarithm of ac onductivity varies with frequency across various temperatures for 10 wt% fly-ash system. Jonscher's universal power law, $\sigma(\omega) = \sigma_0 + A\omega^n$, describes the variation of log σ(ω) with increase in frequency for all temperatures. σ_0 represents dc conductivity, A is the dispersion parameter, and n is the frequency exponent. At low frequencies, the log σ(ω) shows steadiness indicating dc conductivity and deviates from steadiness

for higher frequencies [34]. Dispersion of ac conductivity at critical frequency indicates the relation of conductivy. This critical frequency shifts slightly to higher frequencies with increasing fly ash content. Ac conductivity with frequency is fitted using Jonscher's power law, parameters are calculated and presented in Table 2. It is noted that n is less than one across all temperatures, which supports the hopping of ions from site to site in the sample. The variation of ac conductivity with frequency is explained by using jump relaxation model, which suggests the site to site continuous forward hopping of ions at low frequencies and both forward and backwaed ion hopping at high frequencies [35]. The frequency-dependent conductivity behavior is consistent across all systems.

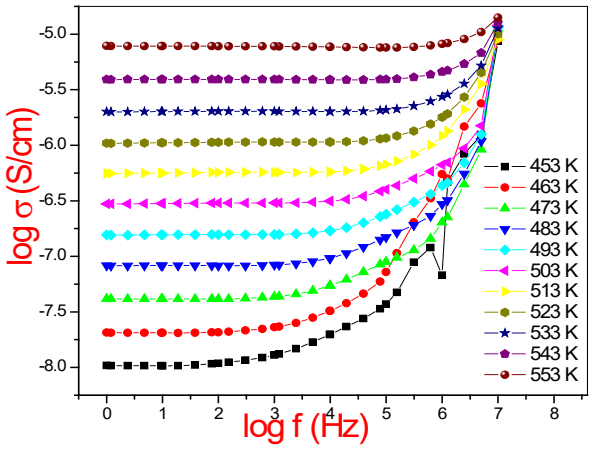

Fig. 9. Variation of ac conductivity with frequency of dispersed system with 10 w/o fly-ash at different temperatures.

Figure 10 shows the dc conductivity, extracted from ac conductivity plots at 1 Hz for host and composite systems.

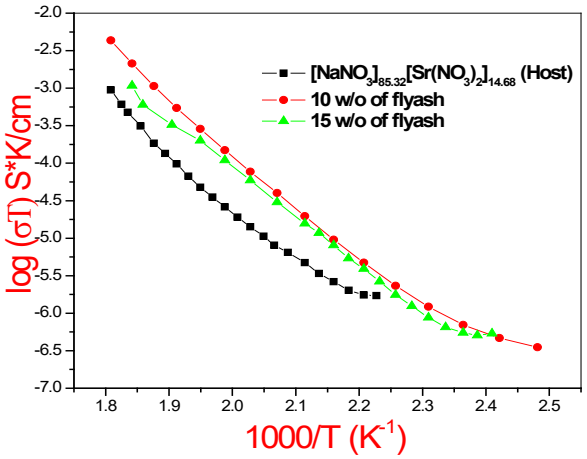

Fig. 10. Variation of dc conductivity (extracted from ac data) with reciprocal temperature.

Figure 11 depicts the temperature dependence of dc conductivity using two probe technique for different fly-ash contents. It is apparent that conductivity rises with increase in temperature for in all systems. Figure 12 shows the variation of dc ionic conductivity (from two probe) with w/o fly-ash at 453 and 523 K The both ac and dc data reveals that the dc conductivity enhancement with fly ash content peaks at 10 wt%, beyond which it begins to decline. This increase in conductivity is mainly due to spreading of host onto the large surface area of fly-ash, which facilitates the formation of an amorphous phase in the sample, as confirmed by all characterization analyses. This amourphous creation occurs when silica disrupts the host's normal crystalline structure, resulting in a network of disordered, glassy material. The semi-crystalline structure is associated with the presence of tiny crystallites, which increases imperfection concentration and thus conductivity [19-22]. The fall in enhancement in conductivity enhancement at greater fly-ash levels is attributed to a reduction in the overall surface area of interaction between the host mixed system and fly-ashdispersoid [36].

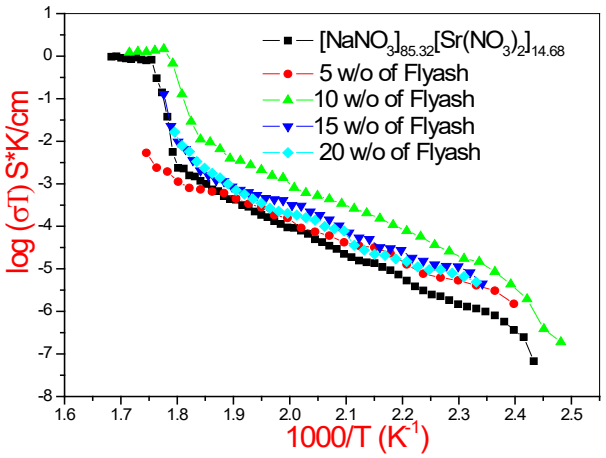

Fig. 11. Variation of dc conductivity (two Probe technique) with reciprocal temperature for with different w/o fly-ash.

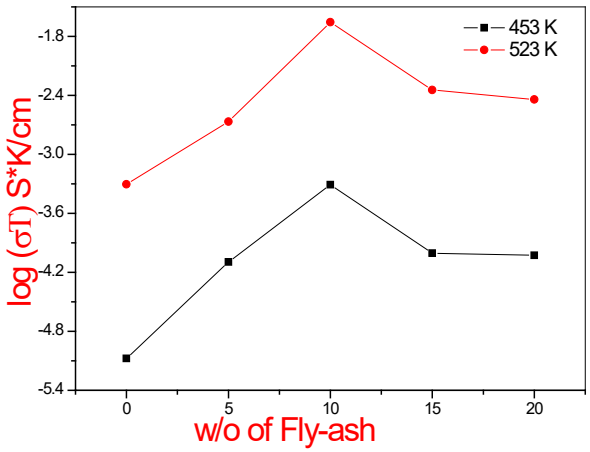

Fig. 12. Variation of dc ionic conductivity with w/o fly-ash at 453 K and 523 K.

Table 2. Parameters (A, n and f_h) of Power law of 10 w/o fly-ash dispersed system at different temperatures.

Temperature(K)	10 w/o fly-ash		
	N	A (S $cm^{-1}rad^{-n}$)	f_h (Hz)
473	0.72	1.44×10^{-11}	4883
493	0.76	9.12×10^{-12}	37144
513	0.78	1.38×10^{-11}	78109
533	1.02	2.18×10^{-13}	312465
543	1.37	2.51×10^{-15}	625000
553	1.4	1.07×10^{-15}	--

4. Conclusions

The broadening and reduction in height of XRD peaks for dispersed fly-ash systems indicate the presence of small crystallites and a reduction in crystallinity of the ionic salt due to significant mechanical stress on the host lattice, leading to the disturbed in crystalline structure.The reduction in intensity of characteristic bands of the host, along with the shift in wavenumber from 1385 to 1365 cm^{-1} and the broadening of the asymmetric stretch of N-O with decreasing intensity, suggests a disordered anion lattice and the existence of an amorphous phase.The noticeable decrease in the endothermic melting peak, and the apparent disappearance of the transition peak in dispersed fly-ash systems, indicate the existence of an amorphous phase.SEM images reveal a disordered host state with no distinct grains in dispersed fly-ash systems.These characterizations confirm the formation of an amorphous phase in the ionic salt.

This amorphous phase is likely located near the host-silica interfaces, possibly interacting with silica aggregates. This interaction is thought to be due to the adsorption of cations from the host onto the silica surface, driven by the nucleophilic (hydroxyl) groups present, as confirmed by FTIR analysis of dispersed systems. This adsorption increases defect concentration in the host, thereby enhancing conductivity. In the amorphous state, the anionic sub-lattice of nitrates is significantly disordered, which contributes to high cationic conductivity. However, with increased fly-ash content, SEM images show particle agglomeration, which reduces the overall surface interaction between the host and the fluy-ash, leading to decreased conductivity.

References

[1] Zhao, Lina, et al., Engineering 24, 172 (2023); https://doi.org/10.1016/j.eng.2021.08.032

[2] Hwang, Jang-Yeon, Seung-Taek Myung, Yang-Kook Sun, Chemical Society Reviews 46(12) 3529 (2017); https://doi.org/10.1039/C6CS00776G

[3] Beniere, F., K. V. Reddy, Journal of Physics and Chemistry of Solids 60(6), 839 (1999); https://doi.org/10.1016/S0022-3697(98)00331-X

[4] Anantha PS, Hariharan K,Mater Sci Eng B, 121, 12(2005); https://doi.org/10.1016/j.mseb.2004.12.005

[5] Madhava Rao MV, Narender Reddy S, Sadananda Chary A, Physica B, 362, 193 (2005); https://doi.org/10.1016/j.physb.2005.02.011

[6] Hu, Chenji, Yanbin Shen, Liwei Chen., Current Opinion in Electrochemistry, 22 5 (2020); https://doi.org/10.1016/j.coelec.2020.05.002

[7] Santhoshkumar, Bandaru, et al., Journal of the American Ceramic Society, 105 (7) 5011 (2022); https://doi.org/10.1111/jace.18463

[8] Zhang, Z., et al., Materials Today Sustainability, 21,100 (2023);

https://doi.org/10.1016/j.mattod.2023.02.027

[9] Sagane, Fumihiro, et al., Journal of power sources, 146 (1-2) 749 (2005); https://doi.org/10.1016/j.jpowsour.2005.03.075

[10] Rao Chintamani Nagesa Ramachandra, Bhartendu Prakash, M. Natarajan, Crystal structure transformations in inorganic nitrites, nitrates, and carbonates, National Bureau of Standards, 1975; https://doi.org/10.6028/NBS.NSRDS.53

[11] Badr, Kamel, J Phys Chem Solids, 41(10),1127 (1980); https://doi.org/10.1016/0022-3697(80)90069-4

[12] Ramasastry C, Murti YVGS, Proc R Soc A, 305(1483), 441 (1968); https://doi.org/10.1098/rspa.1968.0126

[13] Ghadekar SR, Deshmukh BT, J Phys D Appl Phys, 15, 2241(1982); https://doi.org/10.1088/0022-3727/15/11/016

[14] Vijay Kumar T, Swarnalatha R, Sadananda Chary A, Narender Reddy S, Adv Appl Sci Res, 3(5), 2599 (2012).

[15] Kumar, T. V., et al, Journal of Ovonic Research, 19, 6 (2023). https://doi.org/10.15251/JOR.2023.196.643

[16] Masilamani, V., J. Shanthi, V. Sheelarani. International Scholarly Research Notices, 2014 (1) 1 (2014); https://doi.org/10.1155/2014/678567

[17] A.G.S. Kumar, L. Xuejin, Y. Du, Y. Geng, X. Hong, J. Alloys Compd., 798, 467 (2019); https://doi.org/10.1016/j.jallcom.2019.05.227

[18] Zhao L, Wang Y, Chen Z, Zou Y, Physica B, 403, 1775(2008); https://doi.org/10.1016/j.physb.2007.10.004

[19] Uvarov NF, Vanek P, Savionov M, Zelezny V, Studnicka V, Petzelt J, Solid State Ionics 127, 253 (2000); https://doi.org/10.1016/S0167-2738(99)00288-X

[20] Uvarov NF, Hairetdinov EF, Bratel NB, Russ J Electrochem, 29, 1406 (1993)

[21] Uvarov NF, Bohonov BB, Isupov VP, Hairetdinov EF, Solid State Ionics, 74, 15 (1995); https://doi.org/10.1016/0167-2738(94)90432-4

[22] Ponomareva VG, Uvarov NF, Lavrova GV, Hairetdinov EF, Solid State Ionics, 90, 161 (1996); https://doi.org/10.1016/S0167-2738(96)00410-9

[23] J Greenberg, L.J Hallgren, Journal of Chemical Physics, 33 (3), 900 (1960); https://doi.org/10.1063/1.1731284

[24] Foil A. Miller, Charles H, Wilkins, Analytical Chemistry, 24 (8), 1255 (1952); https://doi.org/10.1021/ac60068a007

[25] Parveen Sultana, Sukhen Das, Biswajoy Bagchi, Alakananda Bhattacharya, Ruma Basu, Papiya Nandy, Bulletin Materials Science, 34(7), 1663 (2011); https://doi.org/10.1007/s12034-011-0374-z

[26] S. Ramesh, Liew Chiam Wen, Ionics, 16, 255(2010); https://doi.org/10.1007/s11581-009-0388-3

[27] Silicon dioxide-nano powder, 10-20 nm particle size (BET), 99.5 % trace metals basis, Produc number 637238,CAS number 7631-86-9.

[28] D.J. Rani, A.G.S. Kumar, L. Obulapathi, T.S. Rao, IEEE Transactions on Dielectrics and Electrical Insulation. 26, 1134 (2019); https://doi.org/10.1109/TDEI.2019.007887

[29] Bitra, HC Rao, et al., Digest J. Nanomater. Biostruct., 16, 1173 (2021). https://doi.org/10.15251/DJNB.2021.163.1173

[30] Bitra Hema Chandra Rao, et al., Ferroelectrics Letters Section 48 (1-3) 46 (2021); https://doi.org/10.1080/07315171.2021.1923120

[31] H. C. Rao Bitra, A. V. Rao, A.G.S. Kumar, G. N. Rao, Digest Journal of Nanomaterials and Biostructures, 16 (3), 1173 (2021); https://doi.org/10.15251/DJNB.2021.163.1173

[32] Amodini Mishra, S.N. Choudhary, K. Prasad, R.N.P. Choudhary, Physica B, 406, 3279 (2011); https://doi.org/10.1016/j.physb.2011.05.040

[33] Ved Prakash, S.N. Choudhary, T.P. Sinha, Physica B, 403, 103 (2008); https://doi.org/10.1016/j.physb.2007.08.015
[34] Jonscher AK, J Mater Sci, 13(2), 553 (1978); https://doi.org/10.1007/BF00541805
[35] Dyre JC, Schrøder TB, Phys Status Solidi B, 230, 5 (2002); https://doi.org/10.1002/1521-3951(200203)230:1<5::AID-PSSB5>3.0.CO;2-J
[36] Reddy SN, Chary AS, Saibabu K, Chiranjivi T, Solid State Ionics, 34 (1-2), 73 (1989); https://doi.org/10.1016/0167-2738(89)90434-7